Stellar Convection and Oscillations and their Relationship

SCORe17 in Heidelberg, October 16–20, 2017

Simulation of the small-scale magnetism in main sequence stellar atmospheres

Oskar Steiner[1,2] & *René Salhab*[1]

[1] Kiepenheuer-Institut für Sonnenphysik (KIS), Freiburg i.Br., Germany

[2] Istituto Ricerche Solari Locarno (IRSOL), Locarno Monti, Switzerland

in cooperation with

Svetlana Berdyugina, Bernd Freytag, Paul Rajaguru, and Matthias Steffen

1. Introduction

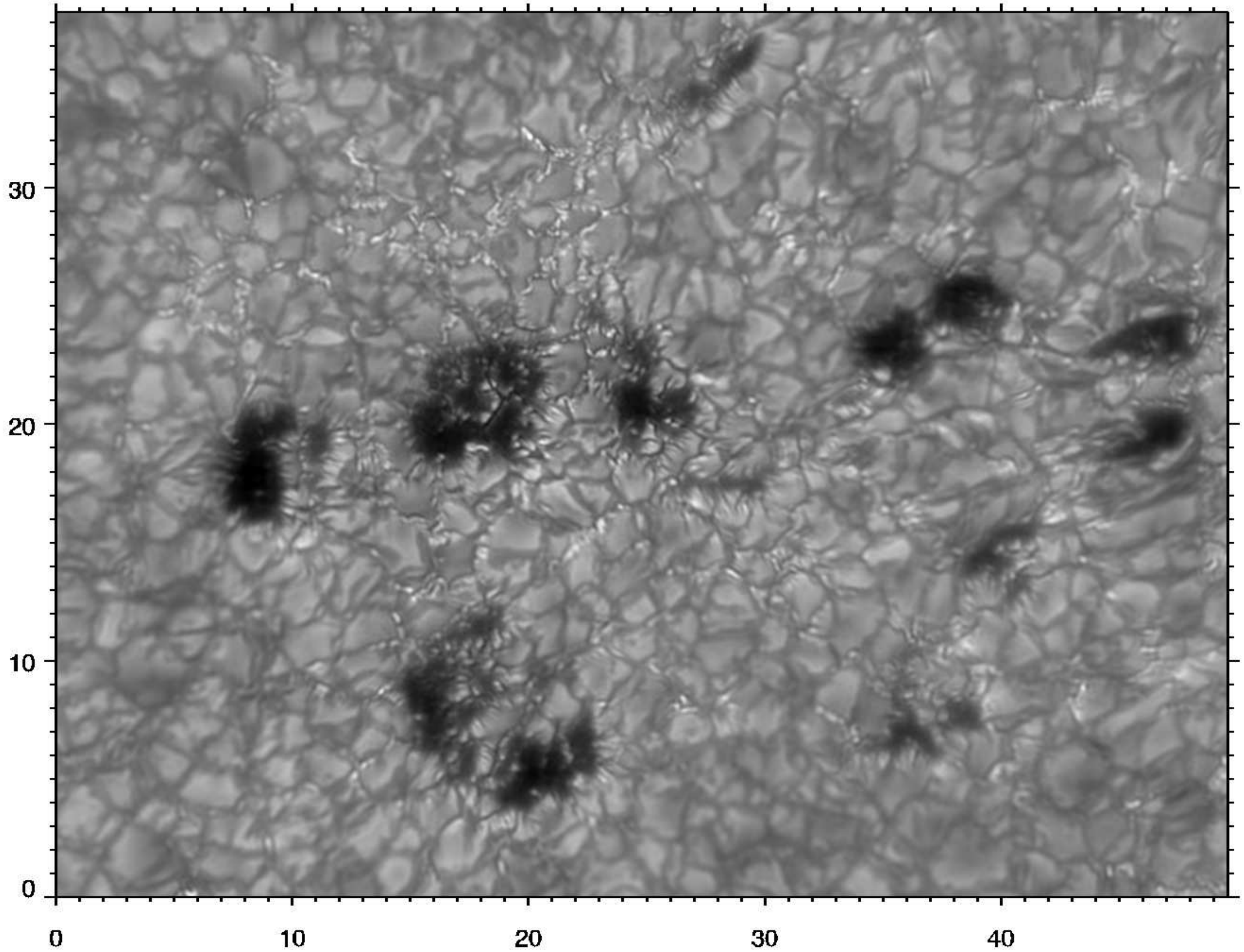

Broadband image ($\lambda = 486$ nm, FOV $49'' \times 37''$) of *solar small-scale magnetic structure*. From “GREGOR first results”: *Schlichenmaier et al., A&A 596, A7*.

SST G-band: Von L. van der Voort

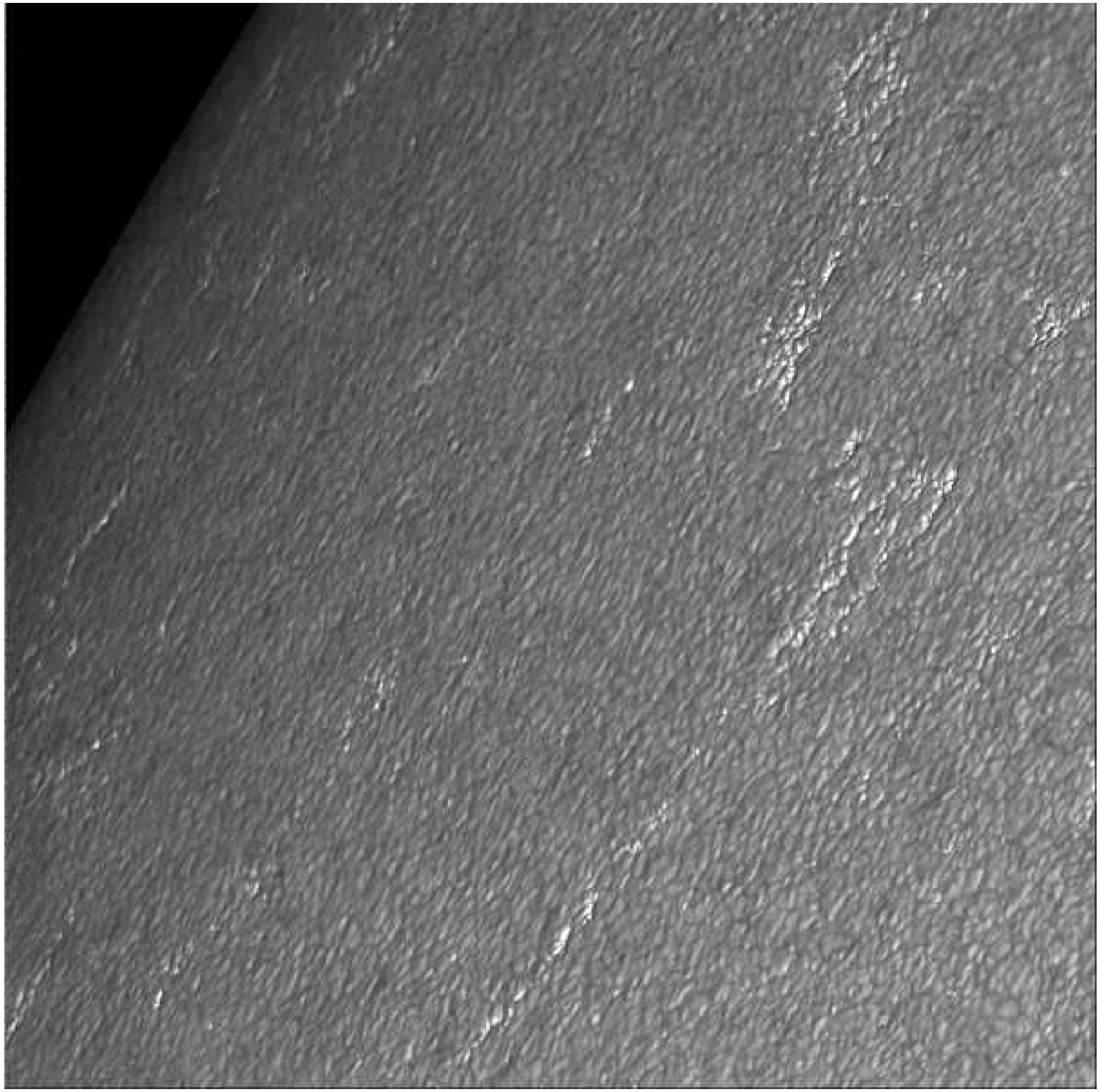

Speckle reconstructed image of *facular regions* taken with the 1 m SST on La Palma in the continuum at 487.5 nm. Field of view approximately $80'' \times 80''$.

From Hirzberger & Wiehr (2005), A&A 438, 1059

The Sun of June 11, 2017

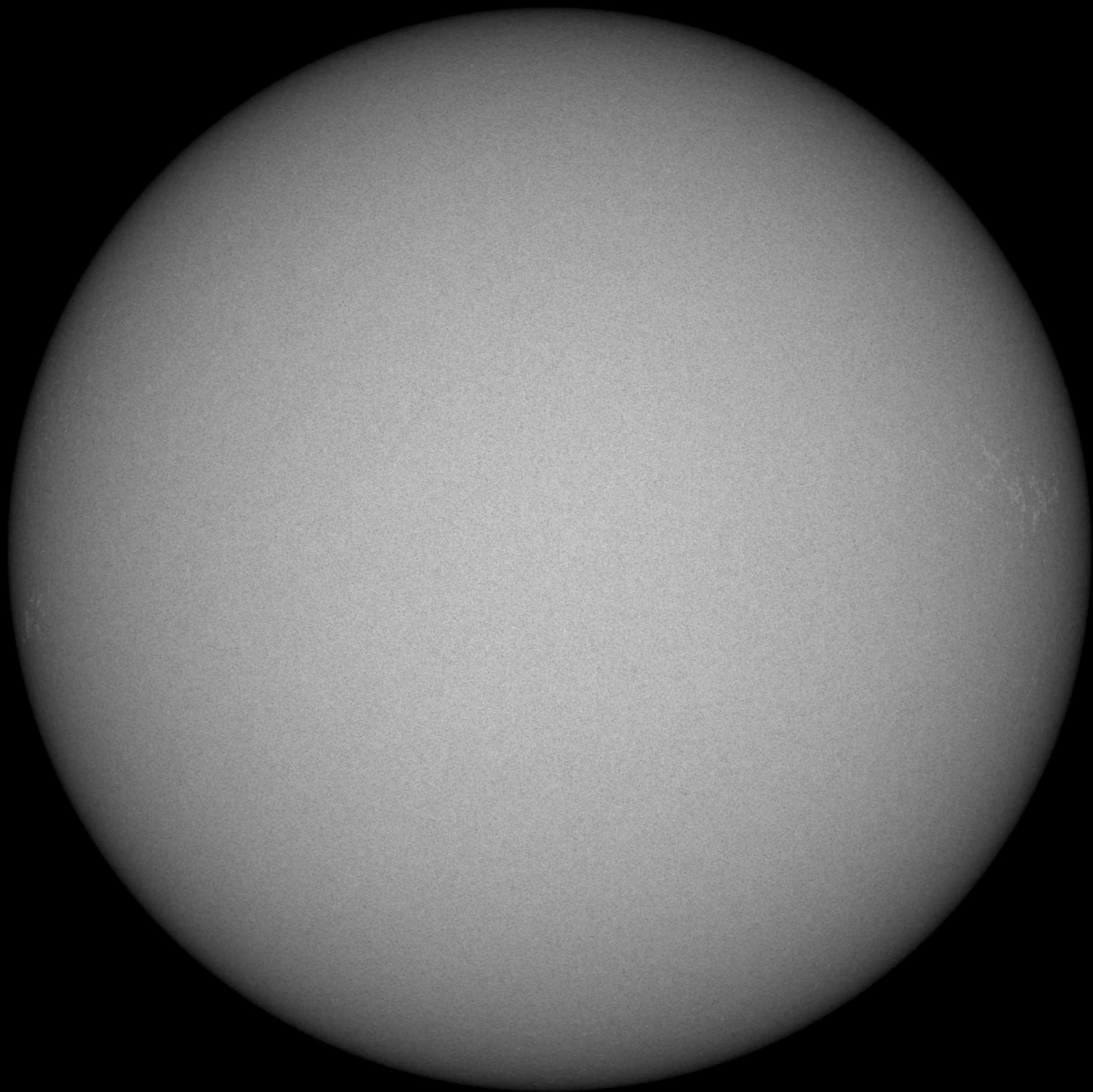

White light image of the Sun. http://sdo.gsfc.nasa.gov/data/

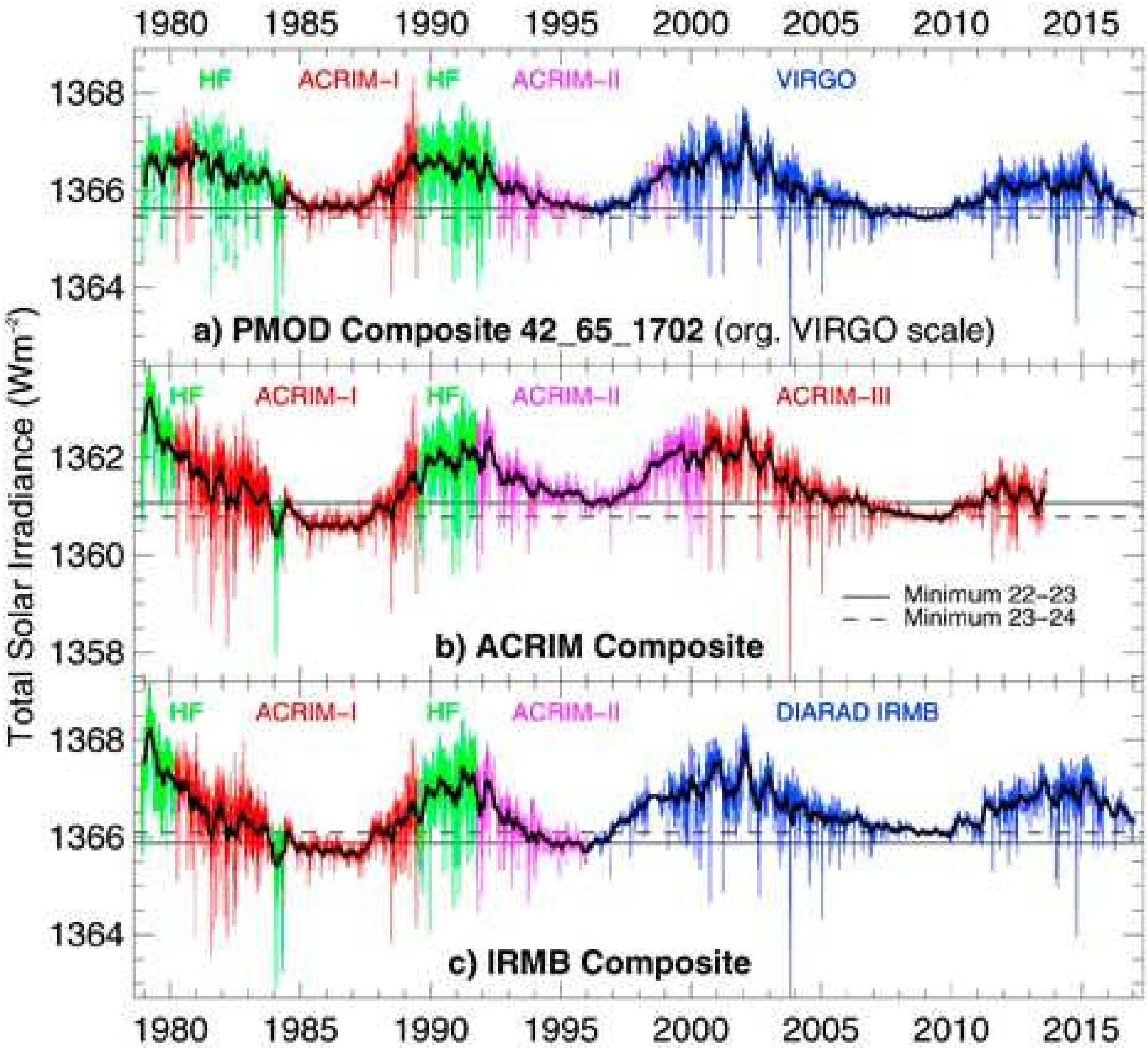

Global consequences of small-scale magnetism

The variability of the solar constant. Three different composites of the *total solar irradiance* (TSI). From http://www.pmodwrc.ch/pmod.php?topic=tsi/composite/SolarConstant

1. Introduction (cont.)

G2.5 V

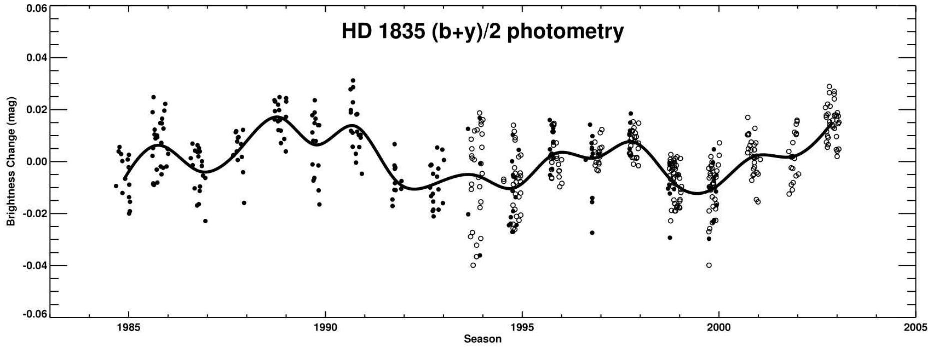

F7 Vn

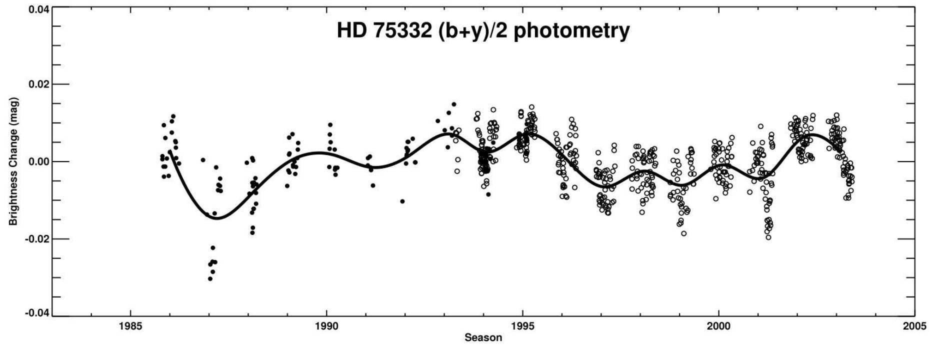

G8 IV-V

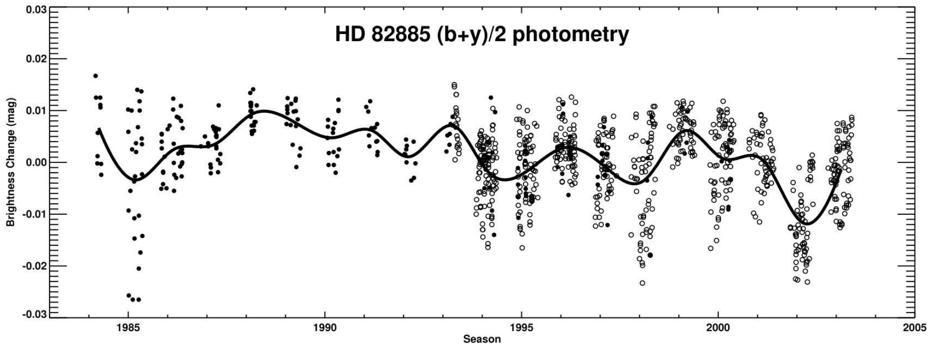

G2 IIIb

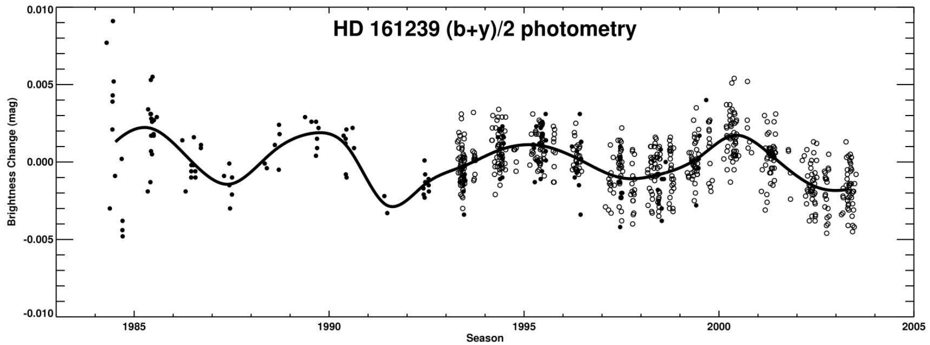

F7 IV

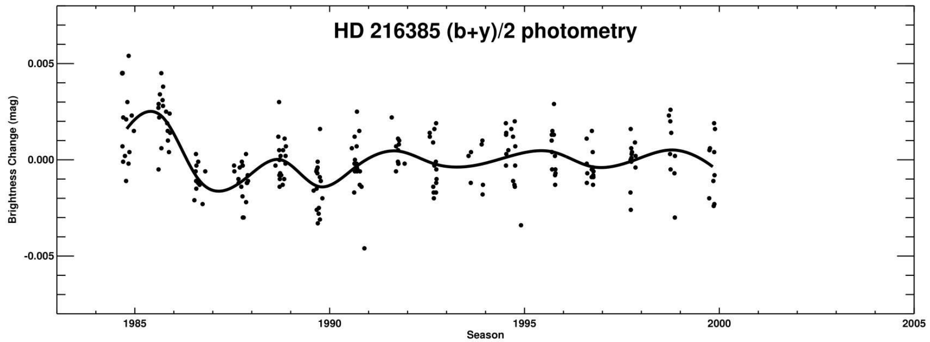

Cyclic photometric variation of Sun-like stars. From *Lockwood et al. 2007, ApJS 171, 260-303*

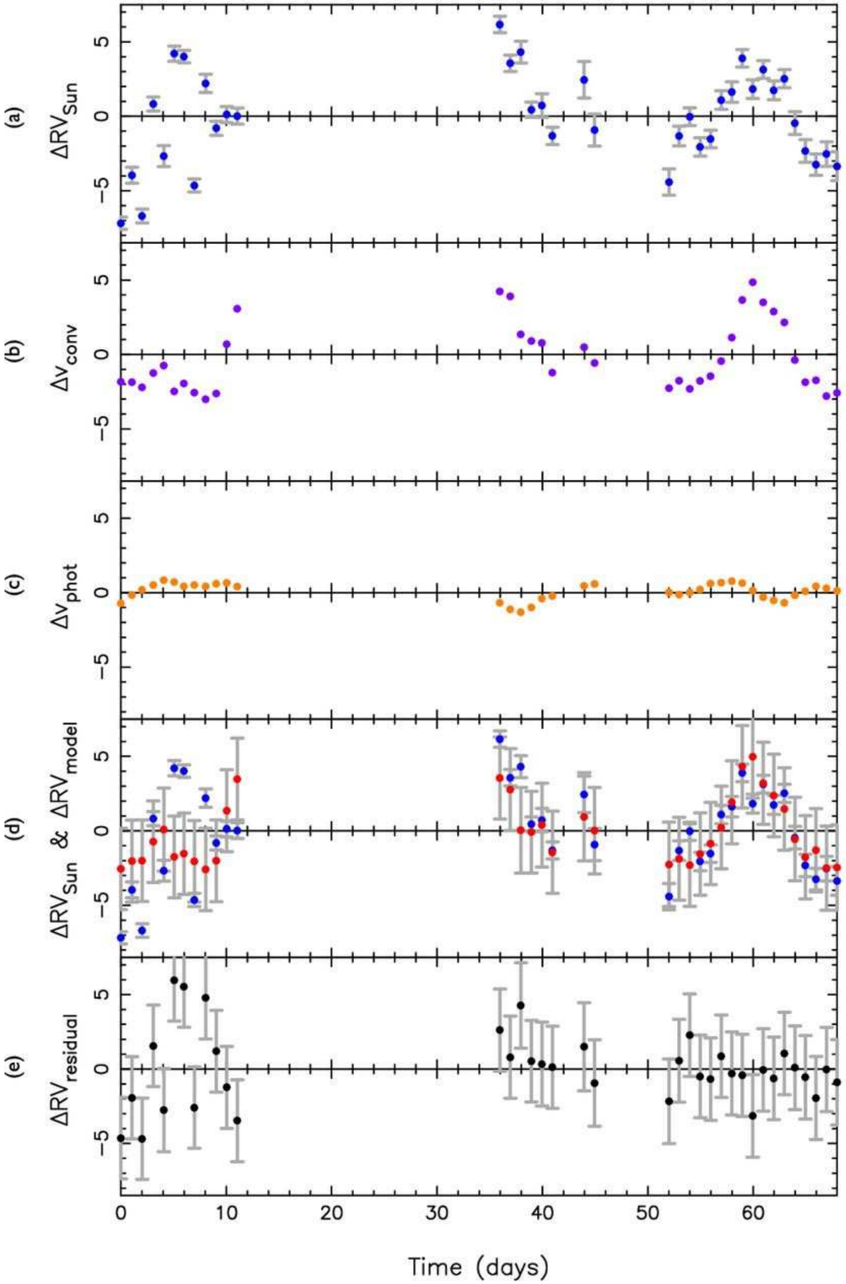

Global consequences of small-scale magnetism

(a) HARPS RV variations of the Sun as a star;

(b) Suppression of convective blueshift, derived from SDO/HMI; rms of 2.4 $\mathrm{m\,s^{-1}}$;

(c) Doppler imbalance due to spots and faculae; rms of 0.17 $\mathrm{m\,s^{-1}}$;

(d) Total RV model (red) on top of the HARPS RV variations (blue);

(e) Residuals.

From *Haywood et al. (2016).*

(See also *Meunier et al. (2010)* for similar results from SOHO/MDI.)

2. The simulations

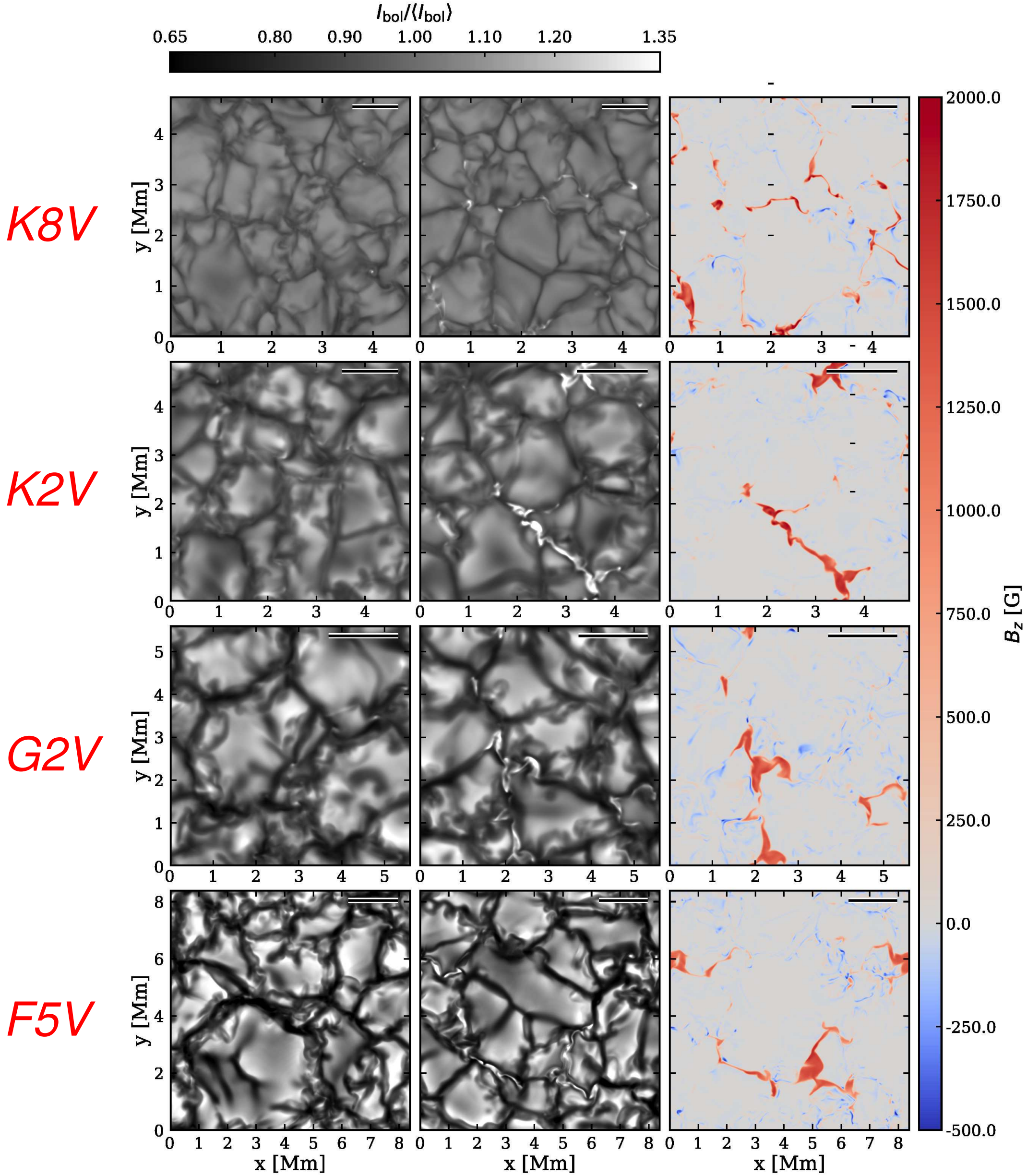

- *"Box in a star" simulations* of the surface layers of four spectral types;
- Each simulation is *run twice*: with and without magnetic fields;
- Initial vertical homogeneous field of *50 G* and *100 G*;
- Multi-group *radiation transfer* using 5 opacity bins;
- Numerical, non-stationary, three-dimensional radiation magnetohydrodynamics using the *CO^5BOLD code*.

spectral type	K8V	K2V	G2V	F5V
$T^*_{\rm eff}$ [K] (nominal)	4000	5000	5770	6500
$\log g$	4.5	4.5	4.44	4.5
$H_p(\tau_{\rm R} = 1)$ [km]	88.1	112.4	149.1	143.2
box depth [N_{H_p}]	10.75	14.17	11.72	11.51
below $\tau_{\rm R} = 1$	3.85	5.77	3.82	6.51
above $\tau_{\rm R} = 1$	6.9	8.4	7.9	5.0
box width [km]	4734	4928	5600	8388
Δz [km]	7	9	12	15
$H_p(\tau_{\rm R} = 1)/\Delta z$	12.6	12.5	12.4	9.5
$\Delta x, \Delta y$ [km]	9	11	14	18
$L_{\rm gran}$ [km]	468	588	772	910
$L_{\rm gran}/\Delta x$	54	53	55	51
box width [$N_{L_{\rm gran}}$]	10.1	8.4	7.3	9.2
$N_{x,y}$	526	448	400	466
N_z	176	276	188	268
$t_{\rm run}$ [min]	633	633	633	633

Some basic properties of the simulation models.

2. The simulations (cont.)

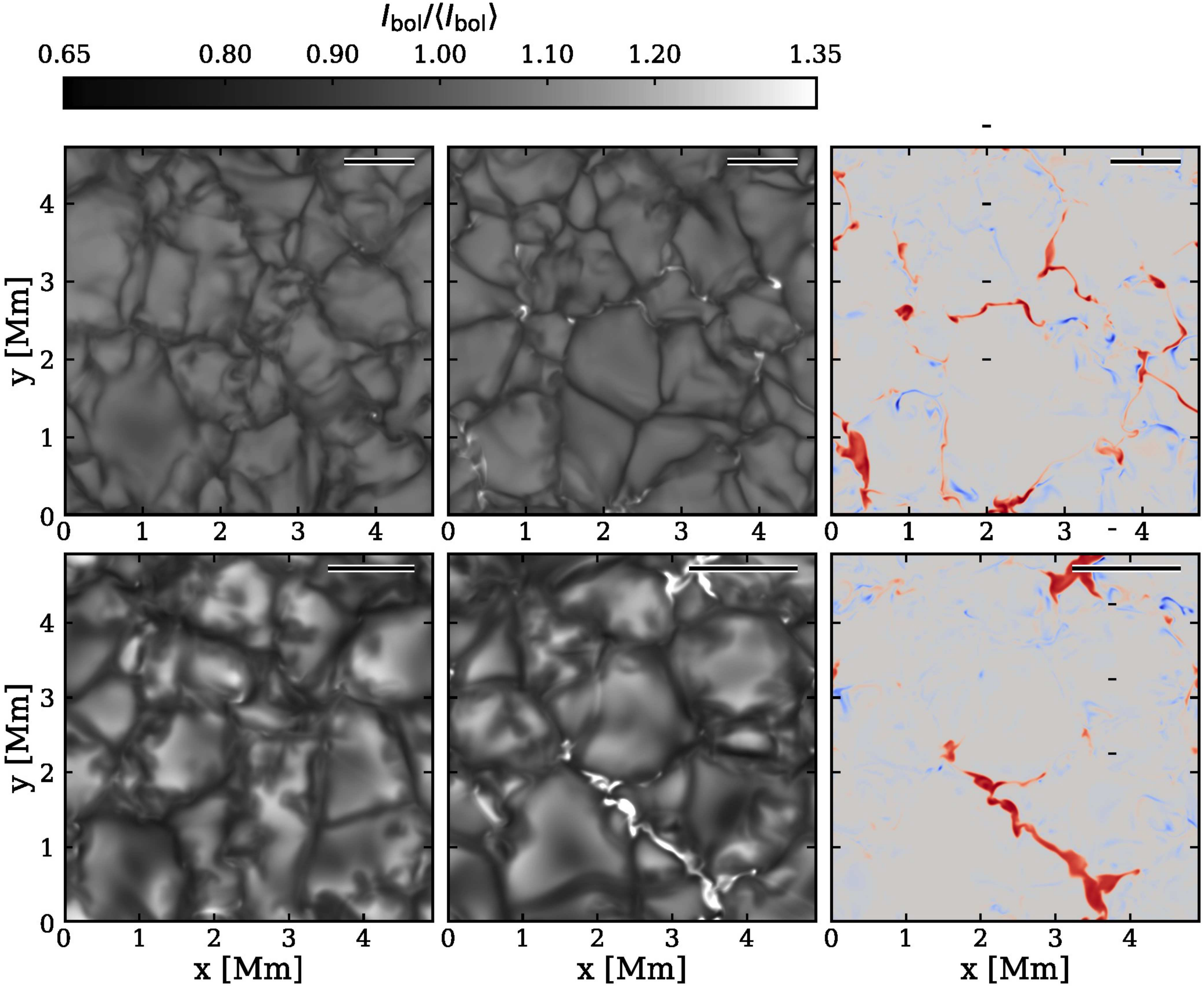

K8V

$c_{bol\,rms} =$ 5.6 %

B0, v50

K2V

$c_{bol\,rms} =$ 9.8 %

B0, v50

From *Salhab et al. (2017)*

2. The simulations (cont.)

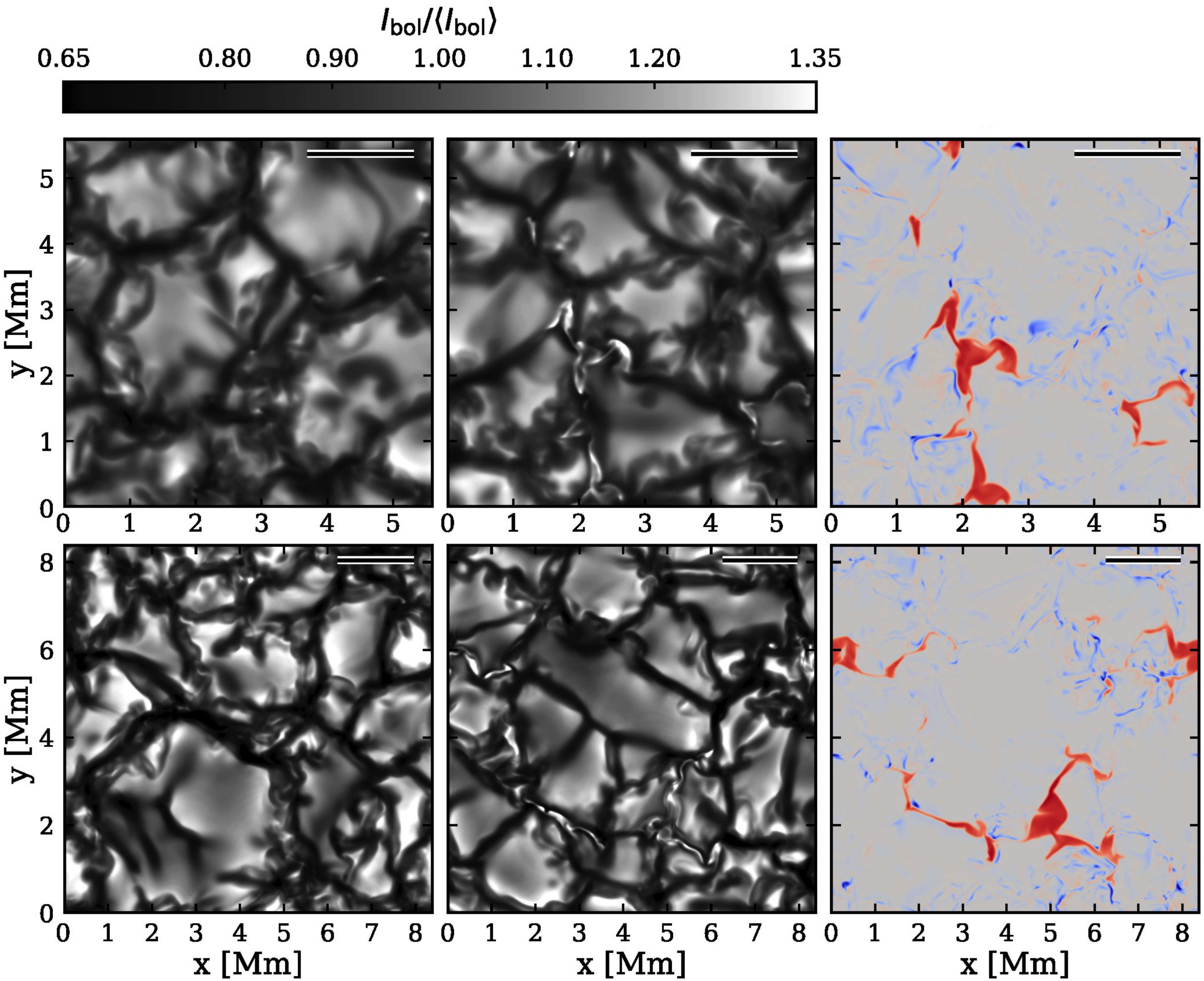

G2V

$c_{\mathrm{bol\,rms}} =$ 15.3 %

B0, v50

F5V

$c_{\mathrm{bol\,rms}} =$ 18.7 %

B0, v50

From *Salhab et al. (2017)*

3. Characteristics of the magnetic flux concentrations

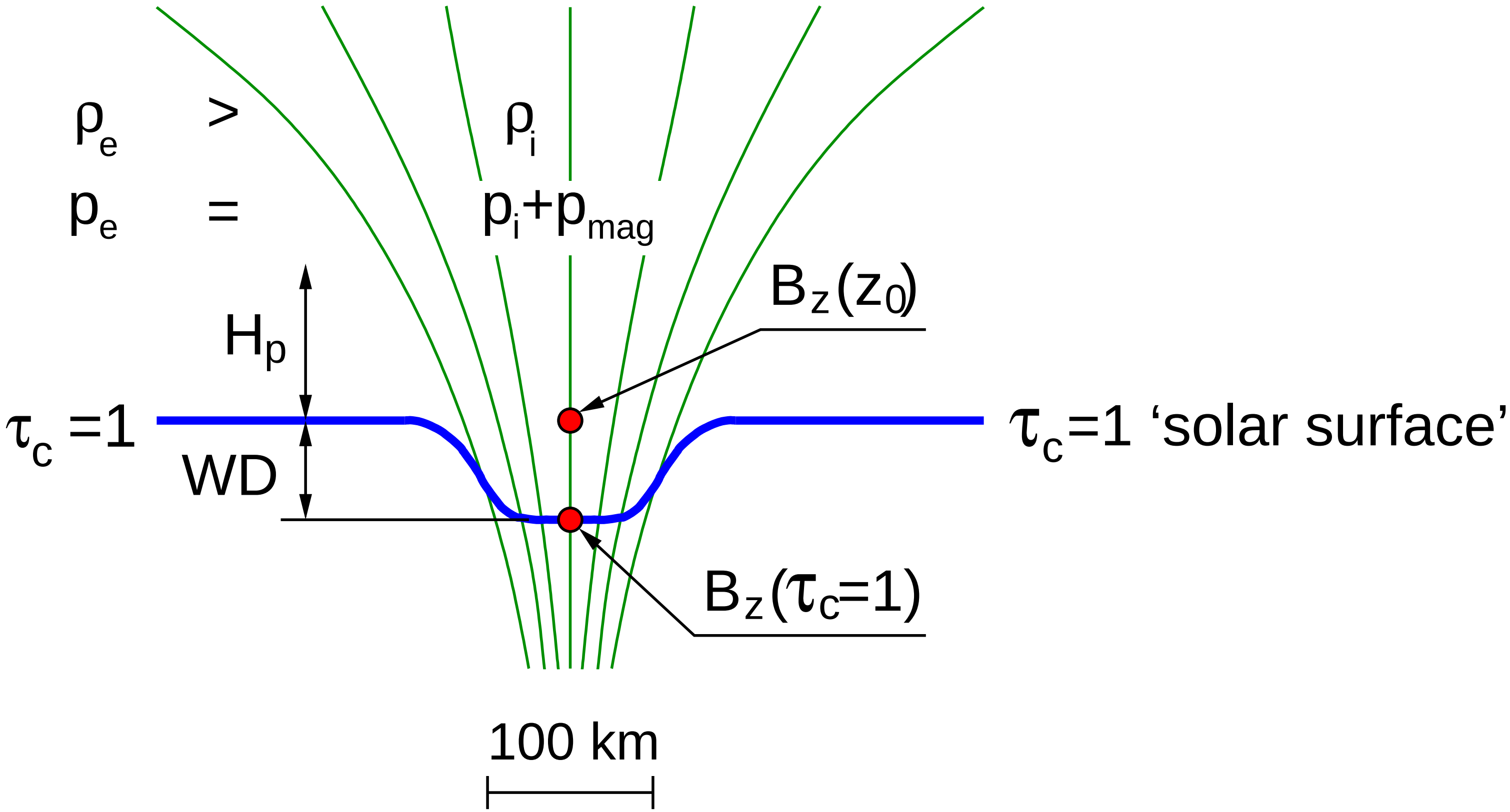

Magnetic flux concentration *(green)* with optical surface $\tau_c = 1$ *(blue)*, and "Wilson depression" WD.

3. Characteristics of the magnetic flux concentrations (cont.)

	spectral type	K8V	K2V	G2V	F5V
	initial B_z [G]	50	50	50	50
1	rms$(B_{z\,\mathrm{MBF}}(z_0))$ [G]	1438 $\pm$40	1358 $\pm$42	1282 $\pm$40	1248 $\pm$32
2	*rms*$(B_{z\,\mathrm{MBF}}(\tau_\mathrm{R}=1))$ *[G]*	1575 $\pm$53	1598 $\pm$93	1480 $\pm$84	1565 $\pm$81
3	max$(\vert B_{z\,\mathrm{MBF}}(z_0)\vert)$ [G]	2204 $\pm$79	1871 $\pm$63	*1739* $\pm$73	*1675* $\pm$85
7	rms$(B_z(z_0))$ [G]	249.9 $\pm$5.5	248.0 $\pm$8.0	238.3 $\pm$7.2	237.9 $\pm$6.5
8	$p_\mathrm{gas}(z_0)$ [kPa]	*26.9* $\pm$0.1	15.2 $\pm$0.1	10.5 $\pm$0.2	*7.52* $\pm$0.2
12	$B_{\mathrm{eq\ th}}(z_0)$ [G]	2596 $\pm$5	1951 $\pm$7	*1614* $\pm$12	1362 $\pm$15
14	$B_{\mathrm{eq\ tot}}(z_0)$ [G]	2681 $\pm$5	2058 $\pm$7	1765 $\pm$11	*1550* $\pm$13
15	$\rho_\mathrm{int}/\rho_\mathrm{ext}(z_0)$ [-]	0.75 $\pm$0.02	0.54 $\pm$0.03	0.46 $\pm$0.04	0.36 $\pm$0.05
16	$\beta(z_0)$ [-]	2.7 $\pm$0.2	1.3 $\pm$0.1	0.74 $\pm$0.1	0.38 $\pm$0.1

• Constant $B_z(\tau=1)\approx 1550$ G. • *Super-equipartition magnetic fields* for F5V and partially for G2V. • Increasing evacuation with increasing T_eff.

3. Characteristics of the magnetic flux concentrations (cont.)

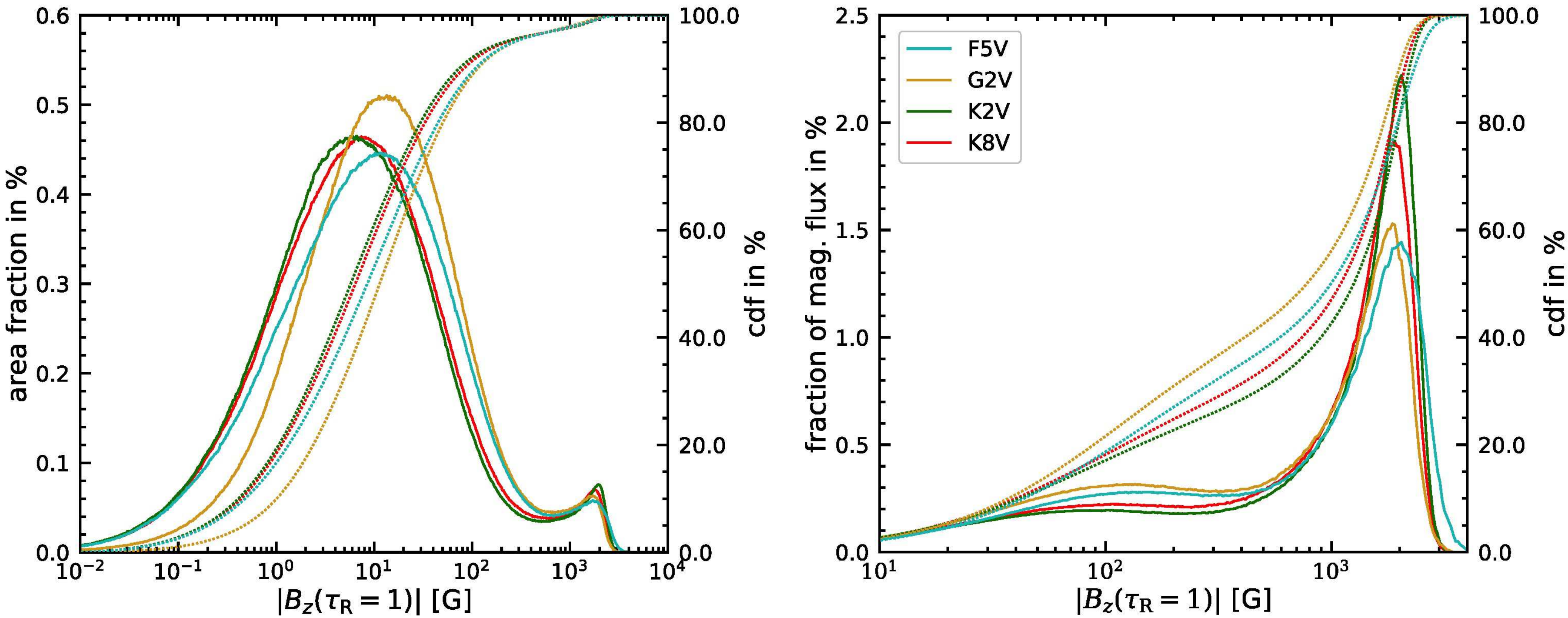

Histograms (*solid curves*) of the absolute vertical magnetic field component on the surface of $\tau_\mathrm{R} = 1$ (*bottom*) of the four (*color-coded*) model atmospheres. *Left:* area fraction per bin of magnetic field strength. *Right:* fraction of magnetic flux per bin of magnetic field strength. *Dotted curves:* cumulative distribution function (cdf).

Conclusion: • $B_{z\,\mathrm{MBF}}(\tau_\mathrm{R}=1) \approx 1550$ [G], fairly *independent of spectral type* • Maximal field strengths can be *superequipartition for F5* but are clearly subequipartition for K8 and K2. • The *evacuation* monotonically *increases with* increasing effective temperature, T_eff.

Conclusions of *Steiner, Salhab, Freytag et al. (2014), PASJ 66, S5*

3. Characteristics of the magnetic flux concentrations (cont.)

Beeck et al. (2015), A&A 581, A42 obtained a similar conclusion for a wider range of spectral types and initial magnetic field strengths.

spectral type	M2V	M0V	K5V	K0V	G2V	F3V	$B_{\rm init}$ [G]
$B_{\rm strong}(\tau = 1)$ [G]	1994	1917	1823	1824	1702	1418	100
	2352	2326	2099	2056	1990	1886	500
$B_{\rm z}(z_0)$ [G]	1948	1922	1758	1662	1536	*1365*	500
$B_{\rm eq\,therm}(z_0)$ [G]	3880	3584	2814	2394	1916	*1387*	500
$B_{\rm eq\,tot}(z_0)$ [G]	3944	3679	2965	2562	2257	1652	500
β	3.1	2.7	1.8	1.4	1.0	0.5	500

Derived from Tables 2 and 3 of Beeck et al. (2015), paper III

4. Radiative properties

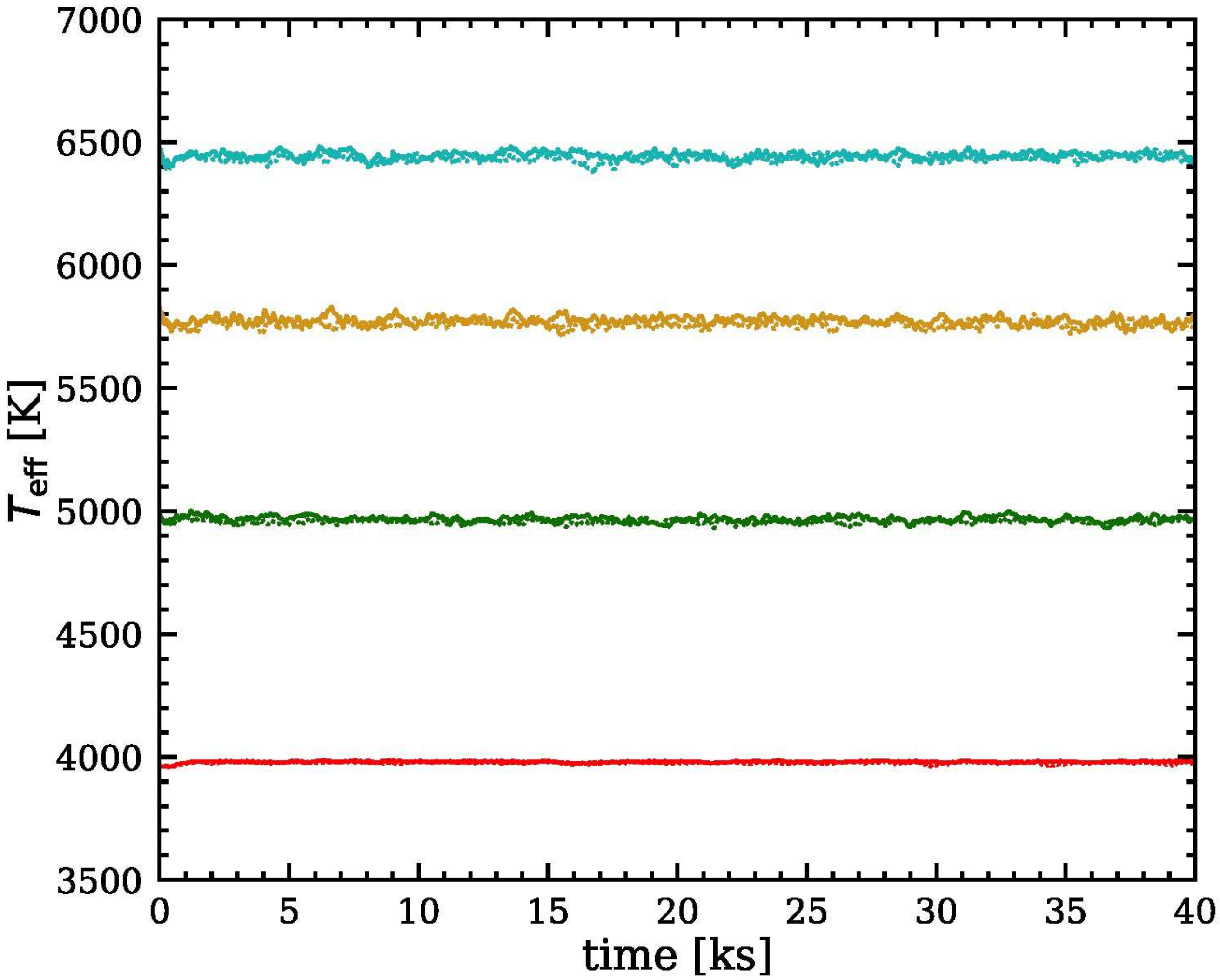

Effective temperature as a function of time of the *non-magnetic models (dotted curves)* and of the *magnetic models (solid curves)* for spectral types *F5V to K8V* from top to bottom.

$$T_{\rm eff} = \sqrt[4]{\langle F_{\rm bol} \rangle_t / \sigma}$$

4. Radiative properties (cont.)

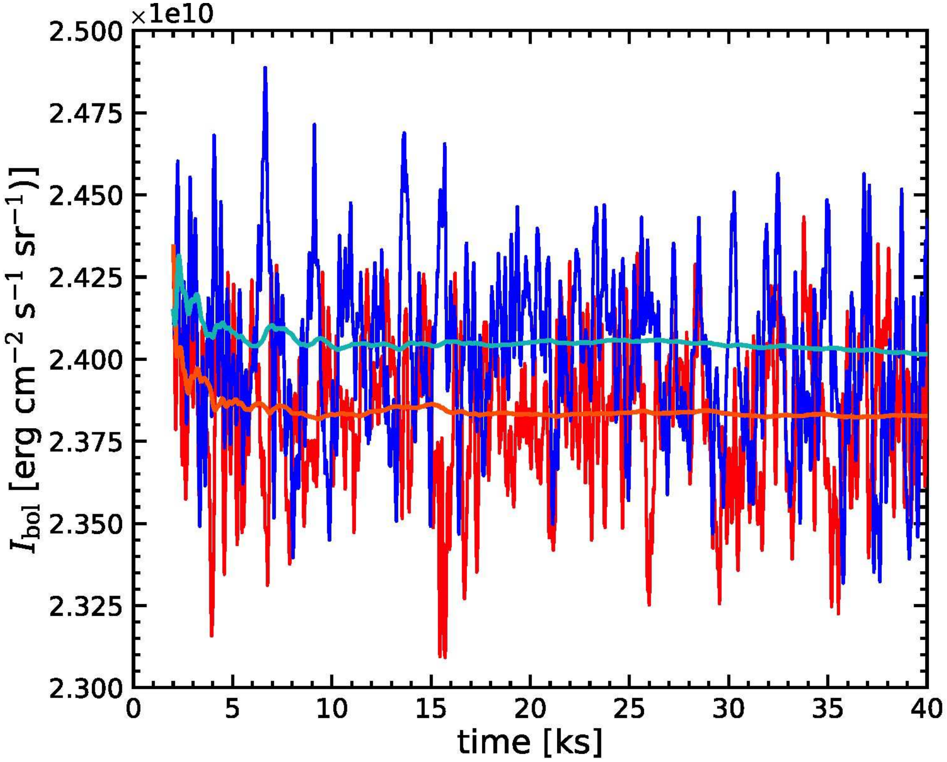

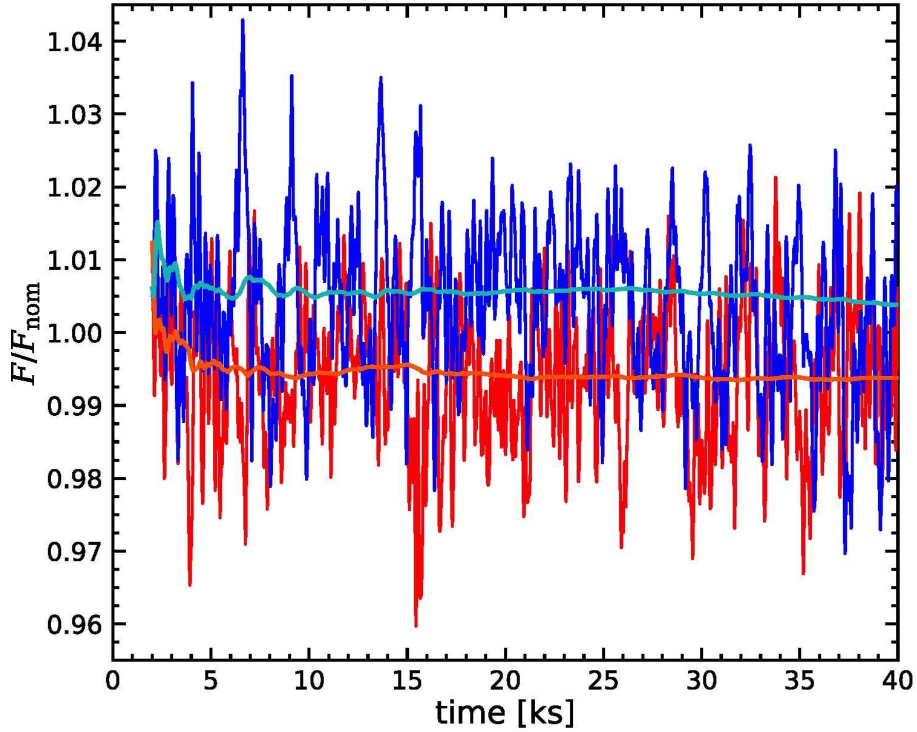

$I_{\rm bol}(t)$ (left) and $F_{\rm bol}(t)$ (right) leaving the computational domain in the vertical direction through the top boundary for the *magnetic* (*blue* curve) and the *non-magnetic* (*red* curve) *solar model (G2V)*. Cyan and orange curves are the *expanding means*.

$$I_{\rm bol}(t) = \langle I_{\rm bol}(\hat{\boldsymbol{z}}, t) \rangle \; ; \qquad F_{\rm bol}(t) = \left\langle \int_{4\pi} I_{\rm bol}(\boldsymbol{n}, t)\, \boldsymbol{n} \cdot \hat{\boldsymbol{z}} \, \mathrm{d}\Omega \right\rangle \, .$$

	spectral type	K8V	K2V	G2V	F5V
	initial B_z [G]	50	50	50	50
25	$\delta_{I_{\rm bol}}$ [%]	0.25 $\pm$0.2	0.68 $\pm$0.9	0.88 $\pm$1.1	0.53 $\pm$0.8
26	$\delta_{F_{\rm bol}}$ [%]	*0.39* $\pm$0.2	*0.86* $\pm$0.9	*1.15* $\pm$1.1	*0.95* $\pm$0.8
27	$\delta_{F_{\rm bol}} - \delta_{I_{\rm bol}}$ [%]	0.14	0.18	0.27	0.42
30	$\mathrm{WD}_{\rm w}$ [km]	60 $\pm$14	139 $\pm$34	232 $\pm$65	388 $\pm$113
31	$\mathrm{WD}_{\rm w}/H_p(\tau_R = 1)$ [-]	0.7 $\pm$0.1	1.3 $\pm$0.3	1.4 $\pm$0.3	2.6 $\pm$0.7
15	$\rho_{\rm int}/\rho_{\rm ext}(z_0)$ [-]	0.75 $\pm$0.02	0.54 $\pm$0.03	0.46 $\pm$0.04	0.36 $\pm$0.05
16	$\beta(z_0)$ [-]	2.7 $\pm$0.2	1.3 $\pm$0.1	0.74 $\pm$0.1	0.38 $\pm$0.1

Radiative surplus of the magnetic over the field-free models, weighted mean *Wilson depression*, and degree of *evacuation* of the flux concentrations.

Magnetic flux sheath in a

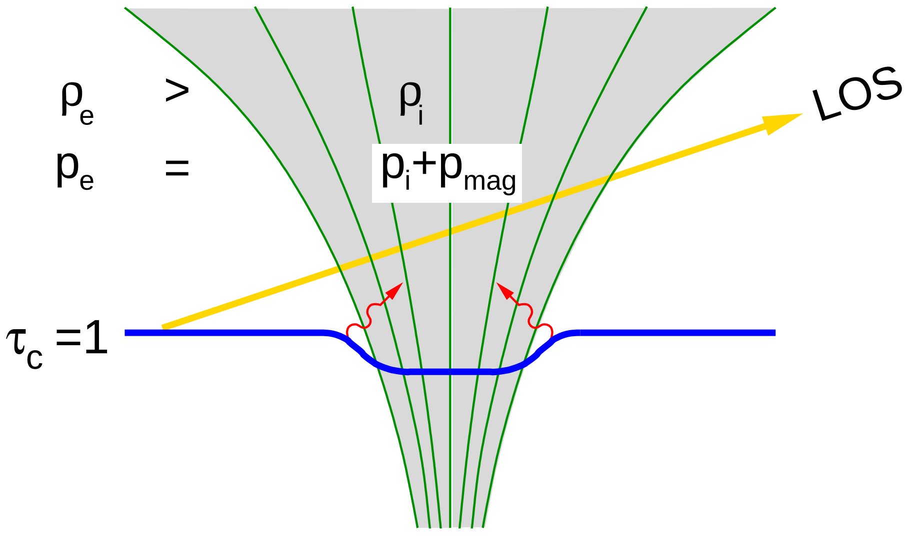

K-type atmosphere

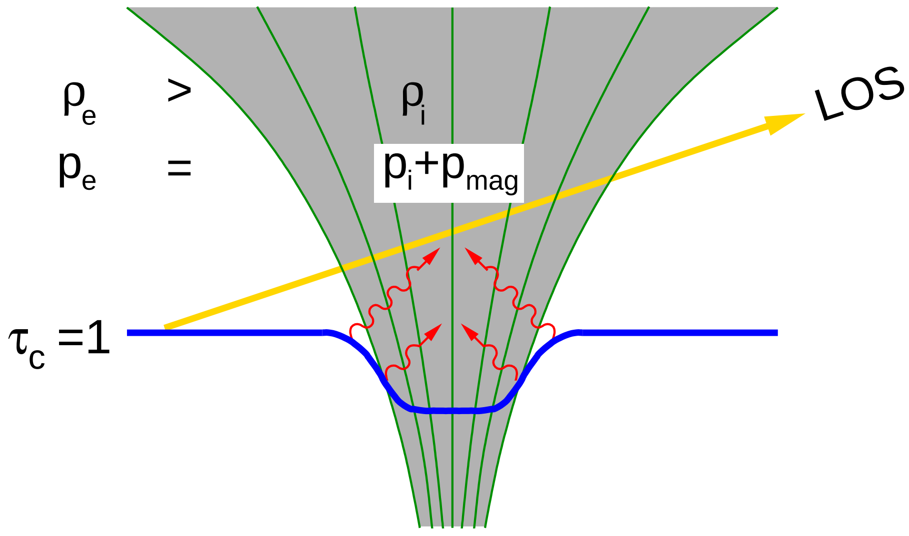

G-type atmosphere.

Bear in mind: It's not the "hot wall" alone that makes faculae.

At least as important is the evacuation of the flux tube atmosphere causing *excess radiative loss from the surroundings* of the magnetic flux concentration proper.

Steiner (2005), A&A 430, 691-700

4. Radiative properties (cont.)

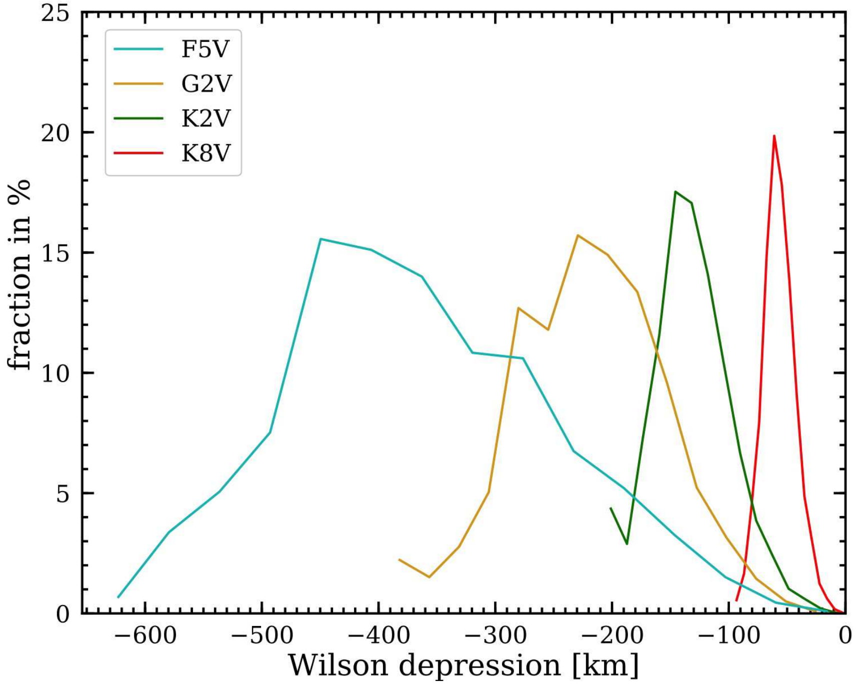

Histograms of the *Wilson-depression* (weighted by the size of the MBF).

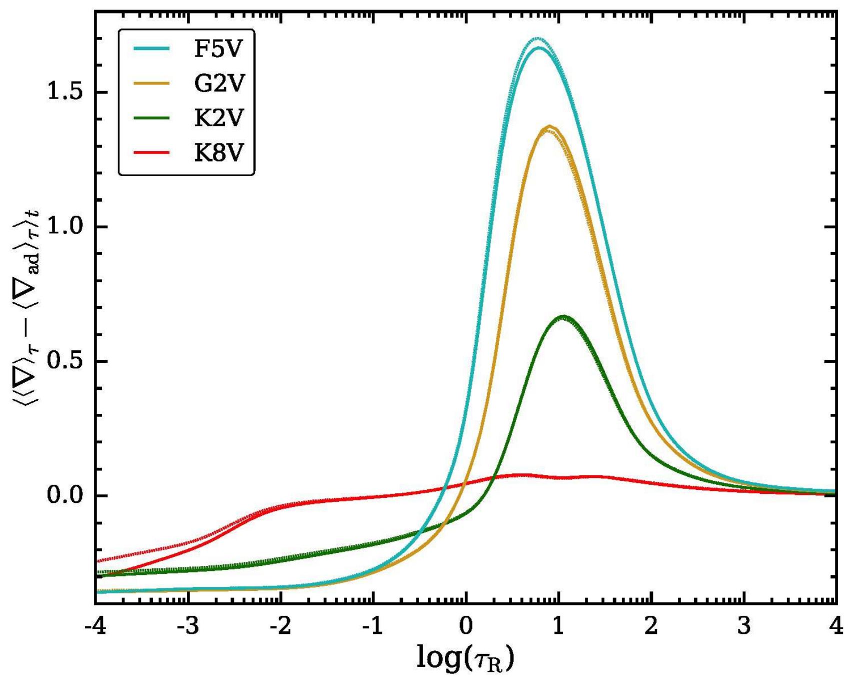

Superadiabaticity $\delta = \nabla - \nabla_{\rm ad}$ as a function of optical depth. The subsurface layers are strongly superadiabatic except for the coolest atmosphere K8V.

4. Radiative properties (cont.)

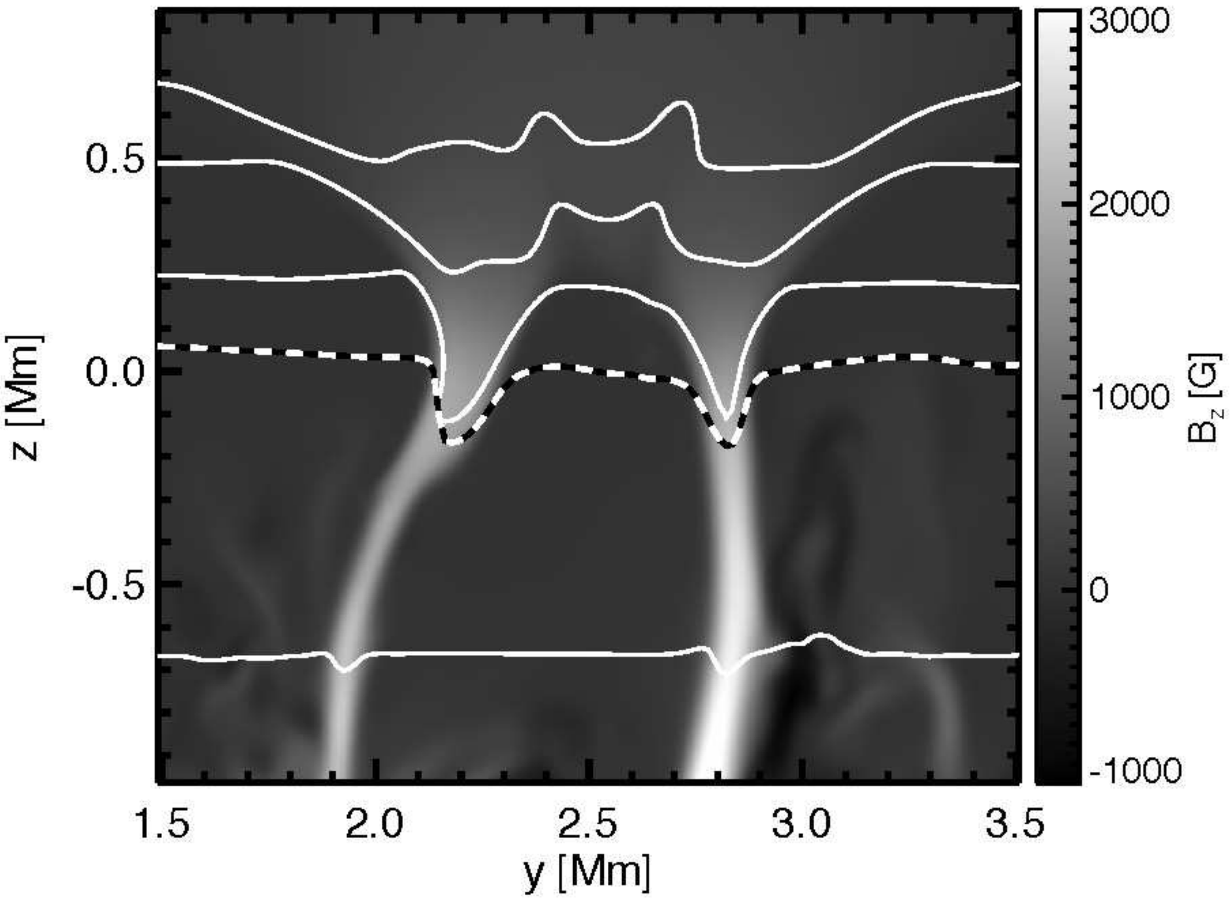

Time instant with two neighboring magnetic flux concentrations of the solar model (G2V). The $\tau_{\mathrm{R}} = 1$ contour (*dashed curve*) shows a *Wilson depression* of ≈ 180 km depth. The *solid white curves* are contours of constant density. Note the substantial *evacuation* in the surface layers.

Conclusion: • For all spectral types considered here, the small-scale magnetic fields produce a *surplus in radiative intensity and flux*. It is most pronounced for G-type and early K-type stars.

• The difference $\delta_{F_{\rm bol}} - \delta_{I_{\rm bol}}$ *is always positive* and monotonically increases with increasing effective temperature, owing to the monotonically increasing Wilson depression and degree of evacuation.

• Small-scale magnetic flux concentrations *form increasingly efficient with increasing* effective temperature $T_{\rm eff}$ owing to the increase in superadiabaticity in the surface layers.

4. Radiative properties (cont.)

Beeck et al. (2015), A&A 581, A43 obtained a similar conclusion in the case of an initial magnetic field of 100 G but wider range of spectral types and initial magnetic field strengths.

spectral type	M2V	M0V	K5V	K0V	G2V	F3V	B_{init} [G]
$\delta_{I_{\mathrm{bol}}}$ [%]	0.07	0.20	0.68	0.10	*1.10*	−0.15	20
	0.20	0.31	1.08	1.38	*1.50*	0.10	100
	−1.77	*−1.03*	1.05	0.87	*0.90*	1.25	500
$\delta_{F_{\mathrm{bol}}}$ [%]	0.22	0.21	0.73	0.16	*1.05*	−0.46	20
	0.33	0.41	1.38	1.82	*2.66*	1.05	100
	−1.08	0.10	3.15	3.76	*7.12*	6.53	500

Derived from Table 1 of Beeck et al. (2015), paper IV

However, *Thaler & Spuit (2014, A&A 566, A11)* found a *radiative deficit of -0.34%* for a solar magnetic simulation with a mean flux density of 50 G. At present, we do not know the origin of this disagreement.

4. Radiative properties (cont.)

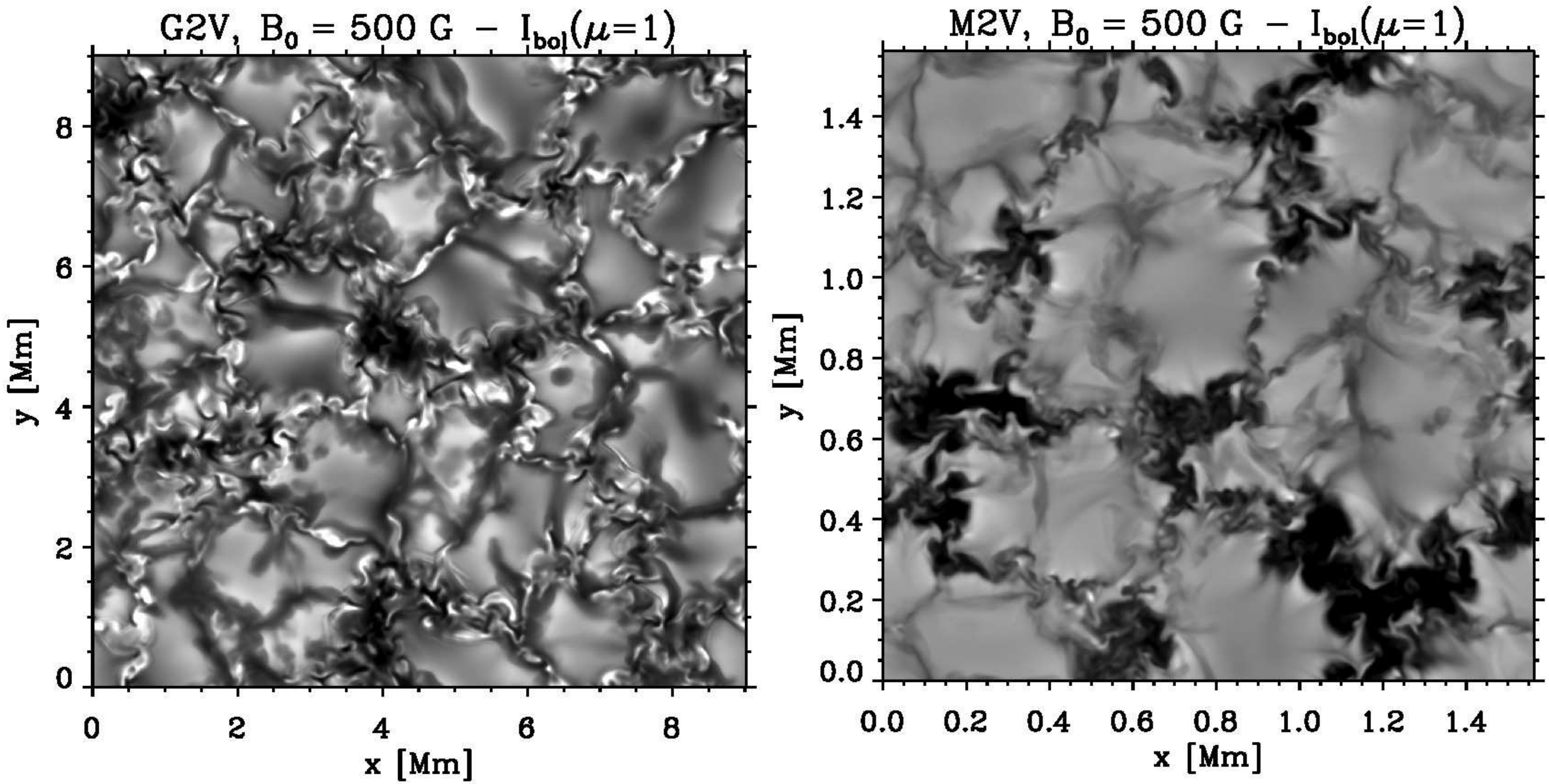

Comparison of a G2V atmosphere with initial magnetic flux density of 500 G *with a M2V model* with the same initial flux. The magnetic filigree conspicuously visible in the G2 model is absent in the spectral type M2 and replaced by dark pore like patches.

From *Beeck et al. (2015, A&A 581, A43)*

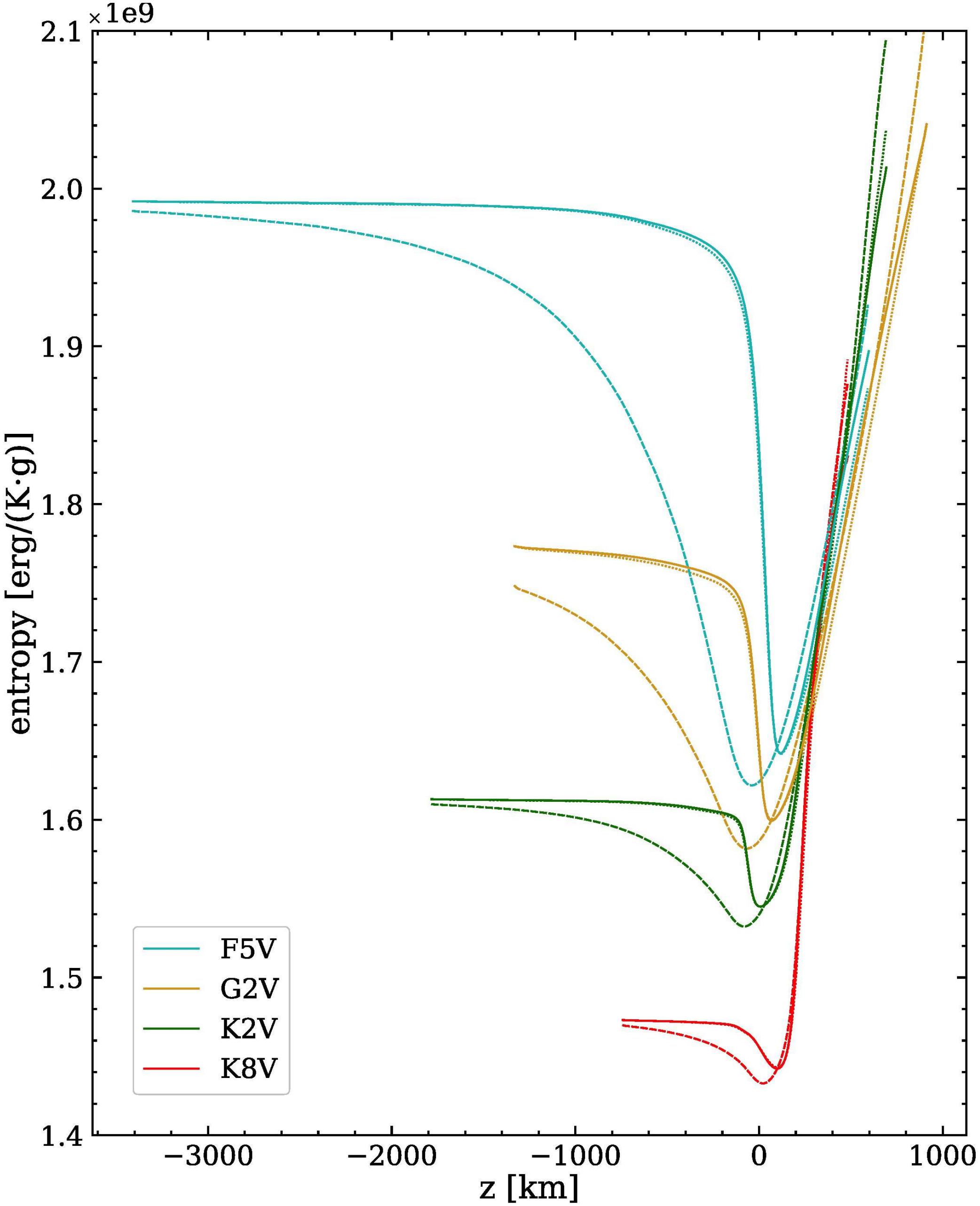

Discussion

The underlying fundamental assumption regarding the lower boundary condition is that the specific entropy of the material entring the computational domain from below the bottom boundary is unaffected by the presence of surface magnetic fields:

$s_{\rm inflow} = \rm const.$

5. Radial velocities

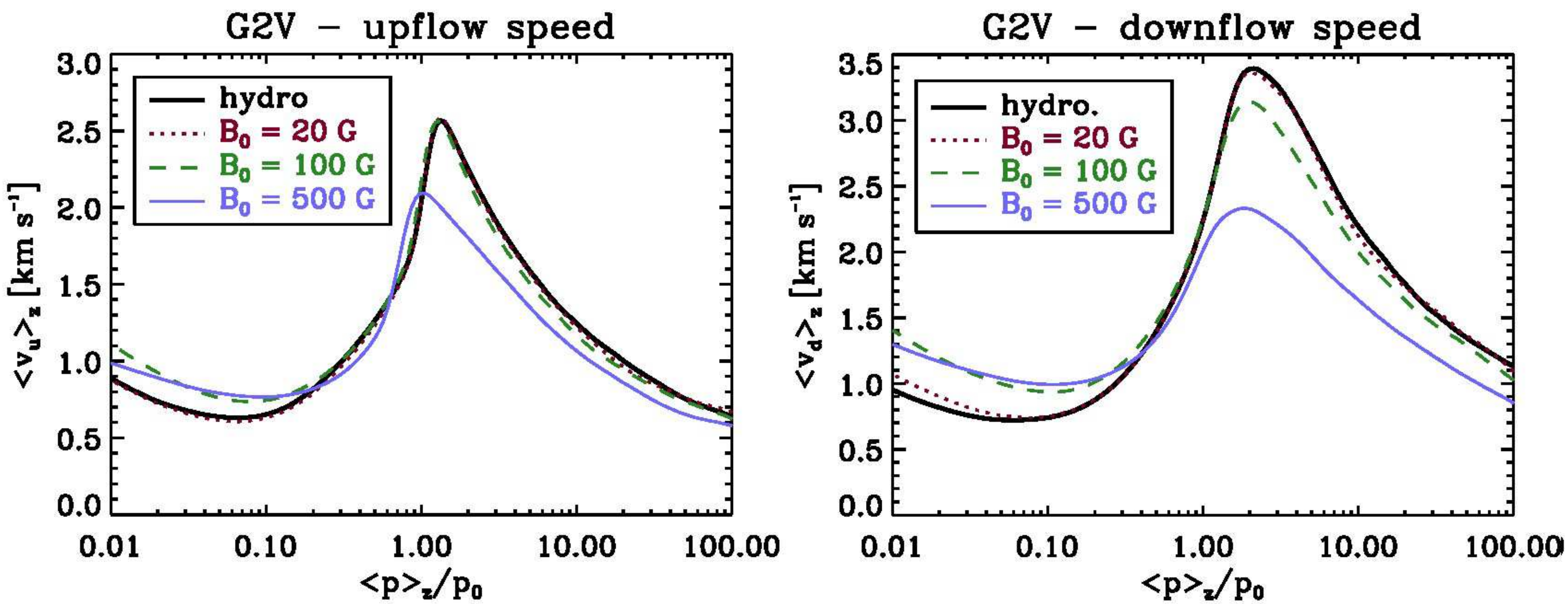

Horizontal mean upflow and downflow speeds in the G2V model with various initial magnetic flux densities. *In the photosphere, the magnetic models tend to have higher downflow velocities*. From *Beeck et al. (2015, A&A 581, A42)*

5. Radial velocities (cont.)

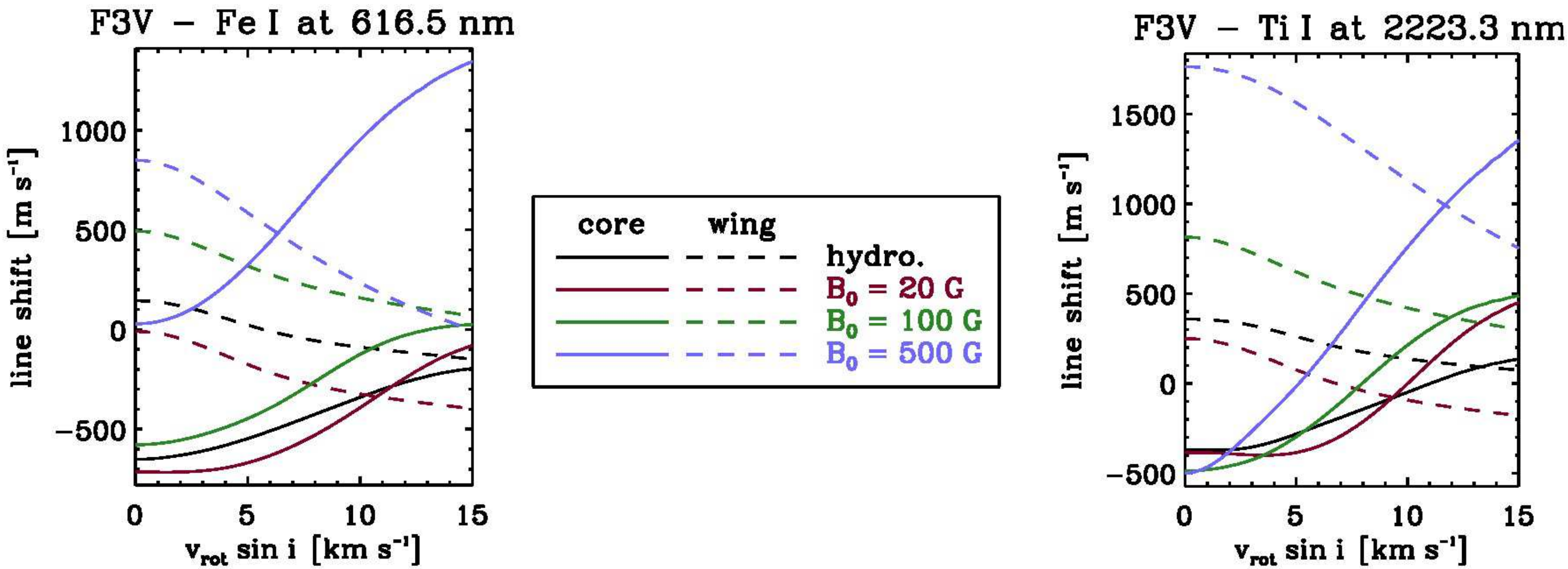

Doppler shift of the line profile cores (solid curves) and wings (dashed curves) of two spectral lines in a F3V model as a function of $V_{\rm rot} \sin i$, where $i = 60^\circ$. Colors indicate different initial magnetic flux densities.

From *Beeck et al. (2015, A&A 581, A42)*

7. Conclusions

- The *surface field strength* of small-scale magnetic elements *stays fairly constant as function of spectral type*. The field reaches thermal *superequipartition* for G2V and earlier spectral types but stays subequipartition for types later than G2.
- The mean vertical *radiative intensity and flux* of the magnetic models is always larger than that of the corresponding field-free model except as for M dwarfs with sufficiently large magnetic flux, which become darker. At mean magnetic flux densities of 50 G to 100 G, the *excess flux is maximal for G2V*.
- The *vertical radiative flux* of the magnetic models is always larger than that of the corresponding field-free model owing to the increase of Wilson depression and degree of evacuation with increasing effective temperature.
- Small-scale magnetic flux concentrations *form increasingly efficient with increasing* effective temperature $T_{\rm eff}$ owing to the increase in superadiabaticity in the surface layers.

Table of content

References

Beeck, B., Schüssler, M., Cameron, R.H., Reiners, A.: 2015, *Three-dimensional simulations of near-surface convection in main sequence stars III. The structure of small-scale magnetic flux concentrations*, , Astron. Astrophys. **581**, A42

Beeck, B., Schüssler, M., Cameron, R.H., Reiners, A.: 2015, *Three-dimensional simulations of near-surface convection in main sequence stars IV. Effect of small-scale magnetic flux concentrations on center-to-limb variation and spectral lines*, , Astron. Astrophys. **581**, A43

Freytag, B., Steffen, M., Ludwig, H.-G., Wedemeyer-Böhm, S., Schaffenberger, W., and Steiner, O.: 2012, *Simulations of stellar convection with CO5BOLD*, , J. Comput. Phys. **231**, 919-959

Haywood, R.D., Collier Cameron, A. Unruh, Y.C. et al.: 2016, *The Sun as a planet-host star: proxies from SDO images for HARPS radial-velocity variations*, , Mon. Not. Roy. Astron. Soc. **457**, 3637-3651

Hirzberger, J. and Wiehr, E.: 2005, *Solar limb faculae*, , Astron. Astrophys. **438**, 1059-1065

Lockwood, G. W., Skiff, B. A., Henry, G. W., Henry, S., Radick, R. R., Baliunas, S. L., Donahue, R. A., and Soon, W.: 2007, *Patterns of Photometric and Chromospheric Variation among Sun-like Stars: A 20 Year Perspective*, , Astrophys. J. Suppl. **171**, 260–303

References (cont.)

Meunier, N., Lagrange, A.-M., and Desort M.: 2010, *Reconstructing the solar integrated radial velocity using MDI/SOHO*, , Astron. Astrophys. **519**, A66

Salhab, R.G., Steiner, O., Berdyugina, S.V., Freytag, B., Rajaguru, S. P., and Steffen, M.: 2017, *Simulation of the small-scale magnetism in main sequence stellar atmospheres*, Astron. & Astrophys. in prep.

Schlichenmaier, R., von der Lühe, O., Hoch, S. et al.: 2014, *Active region fine structure observed at 0.08 arcsec resolution*, , Astron. Astrophys. **596**, A7

Steiner, O., Salhab, R., Freytag, B., Rajaguru, S. P., Schaffenberger, W., and Steffen, M.: 2014, *Properties of small-scale magnetism of stellar atmospheres*, , Publ. Astron. Soc. Japan **66**, S5

Thaler, I., and Spruit, H. C.: 2014, *Brightness of the Sun's small scale magnetic field: proximity effects*, , Astron. Astrophys. **566**, A11